Breast Density Classification using Local Ternary Patterns in Mammograms

Andrik Rampun[1], Philip Morrow[1] Bryan Scotney[1], and John Winder[2]

[1] School of Computing and Information Engineering, Ulster University, Coleraine, N. Ireland, BT52 1SA, UK
y.rampun,pj.morrow,bw.scotney@ulster.ac.uk
[2] School of Health Sciences, Institute of Nursing and Health, Ulster University, Newtownabbey, N. Ireland, BT37 0QB, UK
rj.winder@ulster.ac.uk

Abstract. This paper presents a method for breast density classification. Local ternary pattern operators are employed to model the appearance of the fibroglandular disk region instead of the whole breast region as the majority of current studies have done. The Support Vector Machine classifier is used to perform the classification and a stratified ten-fold cross-validation scheme is employed to evaluate the performance of the method. The proposed method achieved 82.33% accuracy which is comparable with some of the best methods in the literature based on the same dataset and evaluation scheme.

1 Introduction

In the United States (US), an estimated 246,660 new cases of invasive breast cancer were expected to be diagnosed in the US in 2016 with 40,450 women expected to die [1]. Although dense breasts can be inherited genetically, many studies have indicated that breast density is a strong risk factor for developing breast cancer [2–4, 6–12]. Based on the Breast Imaging Reporting and Data System (BI-RADS), there are four major categories used for classifying breast density: (a) predominantly fat, (b) fat with some fibroglandular tissue, (c) heterogeneously dense and (d) extremely dense.

During the last two decades, many breast density classification methods have been proposed in the literature. However, only a few studies have reported accuracy above 80%. The methods of Oliver *et al.* [2] and Parthaláin *et al.* [6] segment the breast region into dense and fatty tissue classes using fuzzy c-means clustering and extract a set of features from each cluster. Feature selection was performed to remove redundant descriptors before feeding them into the classifier. Oliver *et al.* [2] achieved 86% accuracy and Parthaláin *et al.* [6] who used a sophisticated feature selection framework achieved 91.4% accuracy. Bovis and Singh [3] used a combined classifier paradigm and achieved 71.4% correct classification based on a combination of features extracted using the Fourier and Discrete Wavelet transforms in conjunction with first and second-order statistical features. Chen *et al.* [7] compared the performance of local binary patterns (LBP), local greylevel appearance (LGA), textons and basic image features

(BIF) and achieved accuracies of 59%, 72%, 75% and 70%, respectively. Later, they proposed a method by modelling the distribution of the dense region in topographic representation and reported slightly higher accuracy of 76%. Petroudi *et al.* [12] implemented breast density segmentation using textons based on the Maximum Response 8 (MR8) filter bank and reported 75.5% accuracy. He *et al.* [11] achieved an accuracy of 70% using the relative proportions of the four Tabár's building blocks. Muštra *et al.* [5] captured the characteristics of the breast region using multi-resolution of first and second-order statistical features and reported 79.3% accuracy.

The majority results reported in the literature (achieved below 80%) indicate that breast density classification is a difficult task due to a wide variation of tissue appearance in the mammograms. Most of the proposed methods [2–4, 6–12] in the literature extract texture information from the whole breast region whereas most dense tissues are located within the breast fibroglandular disk (FGD_{roi}). In this paper, we propose a method that extracts texture features from the FGD_{roi} only (see Figure 3 later) to obtain more descriptive information. The reminder of the paper is organised as follows: Section 2 presents the technical aspects of our proposed method and; Section 3 discuss experimental results and the quantitative evaluation of the proposed method including quantitative comparisons; and finally Section 4 presents conclusions of this paper.

2 Methodology

We segment the breast region and extract only the FGD_{roi} followed by a simple median filter for noise reduction and extract features to capture the microstructure information from different orientations. The SVM classifier is employed as a classification approach.

2.1 Pre-processing

We used our breast segmentation method [17] to disassociate the breast region from the pectoral muscle and the air background, and extract FGD_{roi} from the breast region. The left most image in Figure 3 shows the estimated fibroglandular disk area. To extract FGD_{roi}, we find B_w which is the longest perpendicular distance between the y-axis and the breast boundary (magenta line). Therefore, the width and the height of the square area of the FGD_{roi} (amber line Figure 3) can be computed as $B_w \times B_w$ with the center located at the intersection point between B_h and B_w lines. B_h is the height of the breast which is the longest perpendicular distance between the x-axis and the breast boundary. B_h is then relocated in the middle of B_w to get the intersection point. The size of the FGD_{roi} varies depending on the width of the breast. For noise reduction, several techniques have been tested such as mean filter, anisotropic diffusion and Gaussian filter, and we found that the median filter using a 3×3 window size produced better results on average.

2.2 Feature Extraction

The Local Binary Pattern (LBP) operators were first proposed by Ojala *et al.* [13] to encode pixel-wise information based on its different mapping tables namely uniform LBP ('u2'), rotation invariant LBP ('ri') and rotation invariant uniform ('riu2'). The Local Ternary Pattern (LTP) operators are among the variants of the LBP operators which have shown promising results in a study conducted by Nanni *et al.* [14]. Both are similar in terms of architecture as each are defined by using a circle and a number of neighbours (see Figure 1). The main difference is that the LTP thresholds the neighbouring pixels into three values -1, 0 and 1 (three-value encoding) using a threshold constant set by the user, whereas the LBP thresholds the neighbouring pixels into two values 0 and 1 (two-value encoding). The LTP decimal value of a pixel (i, j) is given by:

$$LTP_{(P,R)}^{pattern}(i,j) = \sum_{p=0}^{(P-1)} s_{pattern}(g_p)2^p \tag{1}$$

where R is the circle radius, P is the number of neighbours, k is the threshold constant, g_c is the grey level value of the center pixel, p is the neighbouring pixel, g_p is the grey level value of the p^{th} neighbour, and $pattern \in \{upper, lower\}$. Once the LTP code is generated, it is split into two binary patterns (upper and lower patterns) by considering its positive, zero and negative components, as illustrated in Figure 2 using the following conditions

$$s_{upper}(p) = \begin{cases} 1, & \text{if } s(p) > 0 \\ 0, & \text{if } s(p) \leq 0 \end{cases} \tag{2}$$

$$s_{lower}(p) = \begin{cases} 1, & \text{if } s(p) < 0 \\ 0, & \text{if } s(p) \geq 0 \end{cases} \tag{3}$$

The LTP code can be generated using the following conditions

$$s(p) = \begin{cases} -1, & \text{if } p < g_c - k \\ 0, & \text{if } p \geq g_c - k \text{ and } p \leq g_c + k \\ 1, & \text{if } p > g_c + k \end{cases} \tag{4}$$

where $s(p)$ is the p^{th} neighbour containing the LTP code value. In this study we use the uniform LTP ('u2') due to its stability as it is less prone to noise and by considering only uniform patterns making the number of possible LBP labels significantly lower and reliable estimation of their distribution requires fewer samples [16]. To enrich texture information, we extract feature histograms from both upper and lower binary pattern map of the FGD_{roi} at different orientations; $\theta = 0°, 45°, 90°, 135°, 180°, 225°, 270°$, and $315°$ (as shown in Figure 1) resulting in eight histograms. Subsequently, we concatenate these histograms to be a long histogram (representing the occurrences of edges, corners, spots, lines, etc. within

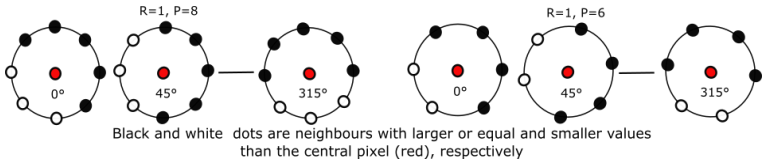

Fig. 1. An illustration of different uniform patterns at different θ and P.

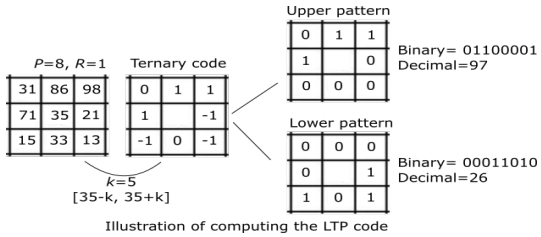

Fig. 2. An illustration of computing the LTP code using $P = 8$ and $R = 1$.

the FGD_{roi}) which will be treated as a feature vector that will be used in the classification phase.

Figure 3 summarises the feature extraction process in this study. Note that, in comparison to the other methods [2–4, 6–12] our proposed method applied the LTP operators only within the FGD_{roi} and features were extracted at eight different orientations.

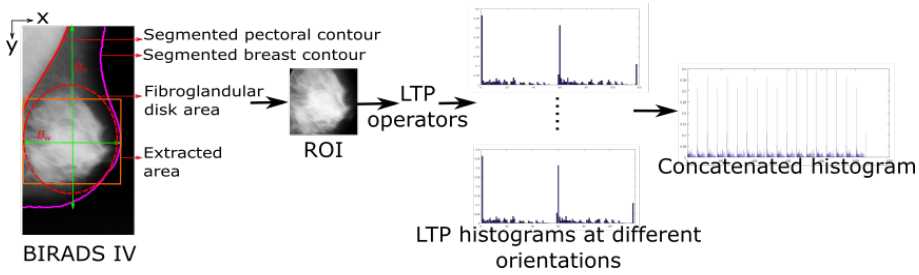

Fig. 3. Summary of feature extraction in our study using the LTP operators.

2.3 Classification

Once the feature extraction was completed, the Support Vector Machine (SVM) was employed as our classification approach. The GridSearch technique was used to explore the best two parameters (complexity (C) and exponent (e)) by testing all possible values of C and e ($C = 1..10$ and $e = 0.1..1.0$) and selecting the best

combination based on the highest accuracy. The SVM classifier was trained and in the testing phase, each unseen FGD_{roi} from the testing set is classified as BI-RADS I, II, III or IV.

3 Experimental Results

To test the performance of the proposed method, we used the well known Mammographic Image Analysis Society (MIAS) database [15] which consists of 322 mammograms of 161 women. Each image contains BI-RADS information (e.g. BI-RADS class I, II, III or IV) provided by an expert radiologist. A stratified ten runs 10-fold cross validation scheme was employed, where the patients are randomly split into 90% for training and 10% for testing and repeated 100 times. The metric accuracy (Acc) is used to measure the performance of the method which represents the total number of correctly classified images compared to the total number of images. The following parameter values for the number of neighbours (P), radius (R), threshold (k) and orientations (θ) were tested to evaluate the performance of the proposed method: (a) $P \in \{5, 6, 7, 8\}$, (b) $R \in \{1, 3, 5\}$, (c) $k \in \{3, 4, 5\}$ and (d) $\theta \in \{0°, 45°, 90°, 135°, 180°, 225°, 270°, \text{and } 315°\}$. In addition, we compare the performance when features are extracted from the whole breast (wb) region versus from the FGD_{roi}.

Table 1 presents the quantitative results when extracting features from the wb region versus from the FGD_{roi}. Note that θ^{ALL} means histograms from the following orientations were concatenated: 0°, 45°, 90°, 135°, 135°, 180°, 225°, 270°, and 315°. Results show that features are more discriminant if extracted only from the FGD_{roi} instead of from the whole breast region. For each case in Table 1, the same parameter settings were used but features were derived from the FGD_{roi} and wb, and at least $3 - 5\%$ difference in accuracy was observed. Our explanation for these results is that in many cases non-fibroglandular disk areas predominantly contain fatty tissues regardless of its BI-RADS class because most dense tissues start to develop within the fibroglandular disk area. Therefore, capturing micro-structure information outside the fibroglandular disk means extracting similar information resulting in less discriminative features across BI-RADS classes. In cases where the non-fibroglandular disk region is dominated by dense tissue the FGD_{roi} also mostly contains dense tissue. For example, Figure 4 shows histograms extracted from the whole breast regions (wb) and FGD_{roi} at $\theta = 0°$ for two different breasts (BI-RADS I and IV). To measure the difference quantitatively, we used the χ^2 distance (d) to measure the difference between these histograms and found that $d = 0.0705$ for H_1^{wb} and H_2^{wb} and $d = 0.122$ for $H_1^{FGD_{roi}}$ and $H_2^{FGD_{roi}}$. This means that H_1^{wb} is more similar to H_2^{wb} than $H_1^{FGD_{roi}}$ and $H_2^{FGD_{roi}}$.

Table 2 shows the classification results for the FGD_{roi} when varying the values of k, P, R and θ. The proposed method achieved the best $Acc = 82.33\%$ using $k = 4$, $P = 6$, $R = 5$ and θ^{ALL}. Experimental results suggest that using a single orientation is insufficient to capture the characteristics of dense and fatty tissues due to multidirectional appearance which is complex and uncertain.

Table 1. Classification results when extracting features from wb versus FGD_{roi}

k	P	R	θ	$Acc(\%)$
4	6	5	θ^{ALL}	**82.33(FGD_{roi})**, 76.94(wb)
5	6	5	θ^{ALL}	80.07(FGD_{roi}), 76.64(wb)
4	8	5	θ^{ALL}	78.18(FGD_{roi}), 77.43(wb)
4	6	7	θ^{ALL}	77.69(FGD_{roi}), 74.08(wb)
4	6	3	θ^{ALL}	76.85(FGD_{roi}), 71.69(wb)
3	6	3	θ^{ALL}	76.18(FGD_{roi}), 71.67(wb)

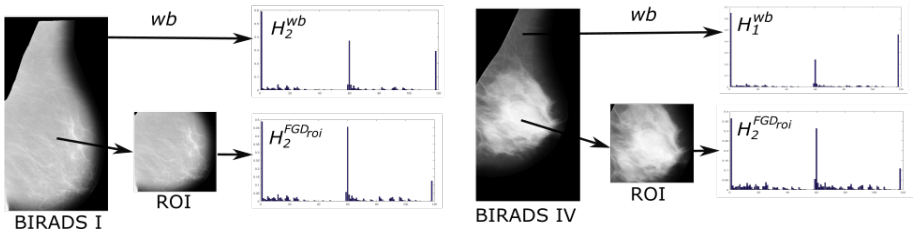

Fig. 4. Histograms extracted from the wb versus FGD_{roi} with BI-RADS class I and IV.

However, using several orientations enable our method to capture complex appearances of the FGD_{roi}. The number of neighbours affects the performance of the extracted features. Results also suggest that the proposed method is highly dependent on the parameter settings in the LTP operators which is the main drawback of our method. However, it can be seen in Table 1 and 2 that the LTP operators can extract robust features for breast density classification in mammograms.

Table 2. Classification results when varying the value of k, P, R and θ (features were extracted from FGD_{roi}).

k	P	R	θ	$Acc(\%)$
-	6	5	θ^{ALL}	79.24($k=3$), **82.33($k=4$)**, 80.07($k=5$), 76.59($k=6$)
4	-	5	θ^{ALL}	76.38($P=5$), **82.33($P=6$)**, 77.04($P=7$), 78.18($P=8$)
4	6	-	θ^{ALL}	72.75($R=2$), 78.17($R=3$), 79.31($R=4$), **82.33($R=5$)**
4	6	5	-	**82.33(θ^{ALL})**, 76.67($\theta=0°$), 74.25($\theta=45°$), 74.07($\theta=90°$), 75.44($\theta=135°$), 76.89($\theta=180°$), 75.22($\theta=225°$), 75.17($\theta=270°$), and 76.61($\theta=315°$)

In comparison to the other methods in the literature, our method achieved 82.33% accuracy which is better than the methods proposed by Muštra *et al.*

[5] (79.3%), Chen *et al.* [7, 9] (59%, 70%, 72%, 75% and 76%), Bovis and Singh [3] (71.4%), and He *et al.* [11] (70%). However, the methods of Parthaláin *et al.* [6] and Oliver *et al.* [2] achieved 91.4% and 86%, respectively. Note that, to minimise bias, these comparisons are based on only those studies that have used the MIAS database [15], four-class classification, and using the same evaluation technique as in this study. Our method outperformed the methods in [3, 4, 7–12] because (a) robust feature extraction operators are used which are able to capture richer micro-structure information using the three-value encoding technique and are less sensitive to noise, (b) the use of FGD_{roi} minimises the texture similarity representation of the breast region hence resulting in more descriptive features across different BI-RADS classes, and (c) we are able to capture a wider range of texture rotation/variation by extracting features from eight different orientations. In breast imaging, deep learning based approaches are becoming popular due to its capability to learn complex appearances especially in the area of segmentation and classification. Despite deemed as a 'black-box' approach study of Kallenberg *et al.* [18] reported their results have a very strong positive relationship with manual ones. Future work would be to employ more texture futures as investigated by the study of Rampun *et al.* [19].

4 Conclusion

In conclusion, we have presented and developed a breast density classification method using the LTP operators applied only within the fibroglandular disk area which is the most prominent region of the breast instead of the whole breast region as suggested in current studies [2–4, 6–12]. By only extracting features from this area, we obtained a set of more discriminative and distinctive texture descriptors across BI-RADS classes. Quantitative comparisons with the existing studies on the same dataset and evaluation technique suggest that the proposed method outperformed most of the current studies in the literature.

Acknowledgments

This research was undertaken as part of the Decision Support and Information Management System for Breast Cancer (DESIREE) project. The project has received funding from the European Union's Horizon 2020 research and innovation programme under grant agreement No 690238.

References

1. Breast Cancer, 'U.S. Breast Cancer Statistics', 2016. [Online]. Available: `http://www.breastcancer.org/symptoms/understand_bc/statistics`. [Accessed:6-Jan-2017]
2. A. Oliver, J. Freixenet, R. Martí, J. Pont, E. Perez, E. R. E. Denton, and R. Zwiggelaar. A Novel Breast Tissue Density Classification Methodology, *IEEE Trans. Inf. Technol. Biomed.*, vol. 12 (1), pp. 55–65, 2008.

3. K. Bovis and S. Singh. Classification of Mammographic Breast Density Using a Combined Classifier Paradigm. *In 4th Int. Workshop on Digital Mammography*, pp. 177–180, 2002.
4. A. Oliver, M. Tortajada, X. Lladó, J. Freixenet, S. Ganau, L. Tortajada, M. Vilagran, M. Sentś, R. Martí. Breast Density Analysis Using an Automatic Density Segmentation Algorithm. *J. Digital Imaging*, Vol. 28 (5), pp. 604–612, 2015.
5. M. Muštra, M. Grgić and K. Delać. A Novel Breast Tissue Density Classification Methodology. Breast Density Classification Using Multiple Feature Selection. *Automatika*, Vol. 53 (4), pp. 362–372, 2012.
6. N. M. Parthaláin, R. Jensen, Q. Shen and R Zwiggelaar. Fuzzy-rough approaches for mammographic risk analysis. *Intelligent Data Analysis*, Vol.14 (2), pp. 225–244, 2010.
7. Z. Chen, E. Denton and R. Zwiggelaar. Local feature based mamographic tissue pattern modelling and breast density classification.*In the 4th Int. Conf. on Biomedical Engineering and Informatics*, pp. 351–355, 2011.
8. A. Bosch, X. Munoz, A. Oliver and Joan Martí. Modeling and Classifying Breast Tissue Density in Mammograms. *Computer Vision and Pattern Recognition (CVPR'06)*, pp. 1552–1558, 2006.
9. Z. Chen, A. Oliver, E. Denton and R. Zwiggelaar. Automated Mammographic Risk Classification Based on Breast Density Estimation. *Pattern Recognition and Image Analysis Volume 7887 of the series Lecture Notes in Computer Science* pp. 237–244, 2013.
10. J. W. Byng, N. F. Boyd, E. Fishell, R. A. Jong and M. J. Yaffe. Automated analysis of mammographic densities. *Physics in Medicine and Biology*, vol. 41(5), pp.909–923, 1996.
11. W. He, E. Denton, K. Stafford and R. Zwiggelaar. Mammographic Image Segmentation and Risk Classification Based on Mammographic Parenchymal Patterns and Geometric Moments. *Biomed. Signal Processing and Control*, vol.6(3), pp.321–329, 2011.
12. S. Petroudi, T. Kadir and M. Brady. Automatic Classification of Mammographic Parenchymal Patterns: A Statistical Approach. *in Proc. IEEE Conf. Eng. Med. Biol. Soc.*, vol. 1, pp. 798-801, 2003.
13. T. Ojala, M. Pietikainen, and T. Maenpaa. Multiresolution gray-scale and rotation invariant texture classification with local binary patterns. *IEEE Trans. Pattern Anal. Mach. Intell.*, vol. 24, no. 7, pp. 971–987, Jul. 2002.
14. L. Nanni, A. Luminia and S. Brahnam. Local binary patterns variants as texture descriptors for medical image analysis. *Artificial Intelligence in Medicine*, vol. 49(2), pp. 117–125, 2010.
15. J. Suckling et al.. The mammographic image analysis society digital mammogram database. *In Proc. Excerpta Med. Int. Congr. Ser.*, pp. 375-378, 1994.
16. A. Hadid, M. K. Pietikainen, G. Zhao and T. Ahonen. Computer Vision Using Local Binary Patterns, Springer London, pp. 13–47, 2011.
17. (under review) A. Rampun, R. J. Winder, P. J. Morrow, B. W. Scotney. Fully Automated Breast Boundary and Pectoral Muscle Segmentation in Mammograms. *Artificial Intelligence in Medicine*, 2016.
18. Unsupervised Deep Learning Applied to Breast Density Segmentation and Mammographic Risk Scoring. *IEEE Trans. on Medical Imaging*, vol. 35(5), pp. 1322–1331, 2016.
19. Computer-aided detection of prostate cancer in T2-weighted MRI within the peripheral zone. *Physics in medicine and biology*, vol. 61(13), pp. 4796–4825, 2016.